Solid-state and solution phase reactivity of 10-hydroxy-10,9-boroxophenanthrene: a model building block for self-assembly processes

Lyndsey M. Greig,[a] Benson M. Kariuki,[b] Scott Habershon,[b] Neil Spencer,[b] Roy L. Johnston,[b] Kenneth D. M. Harris*[b] and Douglas Philp*[a]

[a] *Centre for Biomolecular Sciences, School of Chemistry, University of St Andrews, North Haugh, St Andrews, UK KY16 9ST. E-mail: d.philp@st-andrews.ac.uk*
[b] *School of Chemical Sciences, University of Birmingham, Edgbaston, Birmingham, UK B15 2TT. E-mail: k.d.m.harris@bham.ac.uk*

Received (in London, UK) 7th November 2001, Accepted 23rd January 2002
First published as an Advance Article on the web 7th May 2002

The relative stability of 10-hydroxy-10,9-boroxophenathrene and its electrophilic reactivity are traced through experiment and calculations to the partially aromatic character of the boron-containing heterocyclic ring. The electrophilic reactivity of 10-hydroxy-10,9-boroxophenathrene towards itself in the solid state and towards other nucleophiles in solution is described. The mechanism of the solid-state reaction has been characterised by both X-ray diffraction and thermal analysis. In solution, however, 10-hydroxy-10,9-boroxophenathrene does not react with itself, although it does react rapidly and reversibly with benzylic alcohols in solution, even at low temperatures. This selective and reversible reaction is ideal for use in self-assembly processes.

Introduction

It has been recognised[1] for some time that self-assembly processes are used widely by natural systems in the construction of large, regular superstructures. Familiar examples include the formation[2] of the DNA double helix, the stepwise assembly[3] of the tobacco mosaic virus and the self-regulated construction[4] of the virus bacteriophage T4. These examples illustrate several key principles of self-assembly processes. Firstly, self-assembly processes are highly convergent and are therefore economical in the amount of information required to encode the final structures. In general, self-assembling systems use a relatively small number of simple units to create functionally and structurally complex arrays. If the superstructures are built up from many identical subunits, self-assembling systems typically require only a small set of different interactions to create the final molecular assembly. Finally, molecular recognition using weak non-covalent interactions results in a dynamic process in which all the assembly/disassembly steps are in equilibrium, and therefore reversible. As a result of this reversibility, a degree of proof reading is possible in that the process is self-regulating and can exclude incorrect subunits, to afford the most thermodynamically stable product. Given these advantages, it is desirable for chemists to mimic self-assembling systems of this kind. Indeed, considerable effort has been directed towards the formation of synthetic supramolecular self-assembled architectures in which the assembly process is directed by selective non-covalent interactions, such as hydrogen bonds,[5] or through metal–ligand coordination.[6] There is, however, one major disadvantage to the use of non-covalent interactions in synthetic self-assembly. On formation of the superstructure, a large and unfavourable change in entropy results from the ordering of the components. Formation of non-covalent interactions affords only a small amount of enthalpic stabilisation and, since these interactions are comparitively weak, a significant number of these interactions are required before this stabilisation offsets the entropic loss.

One answer to this problem lies in the use of covalent bonds as a means of constructing large regular assemblies. Covalent bonds are stronger than hydrogen bonds and, hence, a smaller number are required to produce a stable assembly. Traditionally, covalently-linked structures have been synthesised using sequential, kinetically controlled, irreversible reactions. In this manner, relatively large molecules such as vitamin B_{12}[7] and palytoxin[8] have been synthesized. However, the linear formation of such large structures requires a high number of synthetic steps and is extremely time consuming.

To date, the use of covalent interactions in the field of self-assembly has been under-exploited. The use of covalent bond formation in self-assembly processes requires that these bonds form under thermodynamic control, *i.e.* bond formation is reversible, as, for example, in the cases of disulfides[9] or borate[10] esters. One recent example of a system that employs covalent self-assembly has been reported[11] by Sanders and co-workers. The cyclisation of the cinchonidine monomer, methyl-10,11-dihydroquinine-11-carboxylate, is predicted[12] by theory to generate a wide range of oligomers. However, in practice, the trimer is found to be the most stable product. NMR studies show that the conformation of the cinchonidine monomer alters significantly from its ground state conformation during the cyclisation, thus suggesting that the preference to form the trimer is not a result of preorganisation within the monomer, but rather a result of predisposition.[13] Ipaktschi and co-workers have also developed[14] a covalent self-assembly synthetic strategy based upon the directed tetramerisation of quinodimethanes.

Recently, we described[15] (Scheme 1) the covalent self-assembly of bis(hydroxyborazaphenanthrene) **1** to form a dimeric macrocycle **2** by exploiting reversible homoanhydride forma-

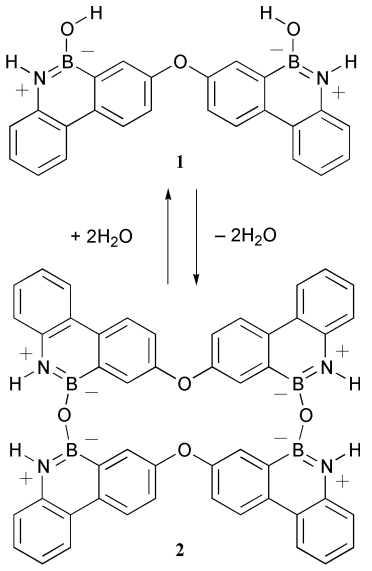

Scheme 1

tion. Although borazaaromatics are attractive building blocks[16] for use in covalent self-assembly processes, their spontaneous formation of homoanhydrides limits their application in this context. In particular, their low reactivity towards other nucleophiles limits the complexity of structures that can be assembled using these building blocks. We therefore identified the corresponding oxygen-containing boroxoaromatics as suitable candidates in our quest to extend the use of boron-containing heteroaromatics in covalent self-assembly processes. Here, we describe in depth the properties, both in solution and in the solid state, of a model boroxoaromatic compound, 10-hydroxy-10,9-boroxophenanthrene, **3**, and reveal features of the reactivity of this compound that make it a potentially useful building block for use in covalent self-assembly processes.

Computational studies

Boroxoaromatics, first described[17] by Dewar in 1959, are a class of compound in which one or more C=C fragments in an aromatic compound have been replaced by the $^{-}B{=}O^{+}$ fragment, and are conventionally represented as aromatic. However, they can also be considered as cyclic boronic esters and there is some debate[18] whether compounds of this type owe their stability to their cyclic structure or to the aromaticity of their boron-containing heterocycles. There is experimental evidence to suggest that they exhibit both aromatic and borate ester properties. For example, the ultraviolet spectrum of 10-hydroxy-10,9-boroxophenanthrene **3** appears to indicate[18d] that it is aromatic, behaving as a protic acid rather than a Lewis acid (the behavior observed for other boronic acids). However, the pK_a of **3** was estimated[18c] to be 9.1, making it one of the strongest boronic acids known and significantly more acidic than several boron–nitrogen heterocycles which have been studied (typical pK_a = 12.0). This observation implies that compound **3** is less aromatic[19] than previously believed. In order to gain some insight into the molecular and electronic structure of boroxophenanthrenes, we carried out a series of *ab initio* electronic structure calculations on compound **3** and the corresponding anhydride, **4**, and, for comparison, on the dimethyl ether–borane complex **5**.

Table 1 Calculated (HF/6-31G(d,p)) bond lengths and Löwdin[19] bond orders for **3**. Data are also provided for **5**, benzene, phenanthrene and ethene for comparison

Compound	Bond	Bond length/Å	Bond order
syn-**3**	Exocyclic O–B	1.35	1.45
	Endocyclic O–B	1.37	1.32
	C–Endocyclic O	1.35	1.17
	C–B	1.55	1.04
anti-**3**	Exocyclic O–B	1.35	1.44
	Endocyclic O–B	1.36	1.33
	C–Endocyclic O	1.35	1.18
	C–B	1.56	1.03
5	O–B	1.72	0.57
	C–O	1.41	1.04
Benzene	C–C	1.39	1.49
Phenanthrene	C–C (9,10)	1.34	1.78
Ethene	C–C	1.32	2.12

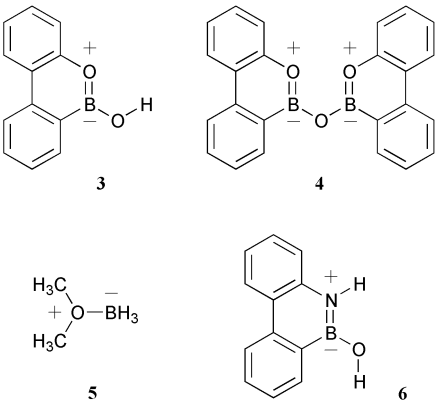

The molecular structure of **3** was calculated at the HF/6-31G(d,p) level of theory. Selected bond lengths and Löwdin[20] bond orders of the geometry-optimised structure of **3** are compared in Table 1 with those of benzene, phenanthrene, ethene and the dimethyl ether–borane complex **5**. The lowest energy structure of **3** is planar, with the O–H bond vector in a *syn* orientation with respect to the endocyclic O–B bond. *syn*-**3** is more stable than *anti*-**3** by around 14.5 kJ mol^{-1} at this level of theory. Data for the *anti* conformation are provided for comparison in Table 1. This preference for the *syn* conformation is in sharp contrast[21] to the corresponding borazaaromatic **6**, in which the O–H bond vector prefers the *anti* orientation with respect to the endocyclic N–B bond. The planarity of the molecule confirms that the oxygen and boron are both sp^2 hybridised and the endocyclic O–B Löwdin bond order (1.32) suggests that this bond has significant π-character. The existence of π-type bonding is illustrated by the calculated HOMO of **3** (Fig. 1), which shows clearly the O–B π-orbital overlap. The endocyclic and exocyclic O–B bond lengths (1.37 and 1.35 Å, respectively) are significantly shorter than the O–B single bond in the dimethyl ether–borane complex **5**

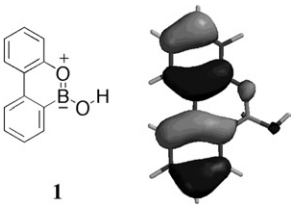

Fig. 1 Representation of the HOMO of **3**, calculated at the HF/6-31G(d,p) level of theory. The molecular structure of **3** is provided in the same orientation for comparison.

Table 2 Calculated (HF/6-31G(d,p)) natural atomic occupancy (NAO) of p_z orbitals of selected atoms in **3**. Data are also provided for benzene for comparison

Compound	Atom	NAO (p_z)
syn-**3**	Exocyclic O	1.82
	B	0.39
	Endocyclic O	1.68
Benzene	C	1.10

(1.72 Å). Interestingly, the bond order of the exocyclic B–O bond in **3** (1.45) suggests that it also has considerable π-character. For a partial π-bond to exist between the B atom and the exocyclic O atom, the hybridisation of the oxygen atom must be sp^2, and the calculated C–B–O and B–O–H angles (126.6 and 115.5°, respectively) indeed demonstrate that the hybridisation of the oxygen atom is closer to sp^2 than sp^3.

The existence of O → B π-donation is supported further by the calculated natural atomic occupancy (Table 2) of the p_z orbital on boron (0.39). However, the occupancy is only half the value (1) that would be expected for an atom in a π-system, such as benzene. Since the boron p_z orbital is only partially occupied, the boron atom may be expected to be somewhat electrophilic. This electrophilic character is demonstrated clearly by considering the electrostatic potential (ESP) surface of **3**. The ESP surfaces on the oxygen and carbon atoms are all minima (Table 3), and are comparable with the carbon atoms of benzene (−84 kJ mol^{-1}) whereas the ESP surface on the boron is a maximum (+98 kJ mol^{-1}). This observation demonstrates that, although there is considerable O → B charge transfer in the π-system, it is outweighed by the B → O charge transfer in the σ-framework. The electropositive surface on the boron, when considered together with the partially occupied p_z orbital, suggests that the boron atom should be reasonably electrophilic.

Synthesis

The synthesis of 10-hydroxy-10,9-boroxophenanthrene **3** (Scheme 2) was carried out using an adaptation of the method described[18d] by Dewar. A solution of 2-phenylphenol in dry diethyl ether was treated with boron trichloride in hexanes at low temperature, forming the corresponding oxoborondichloride **7** *in situ*. Lewis acid-catalysed cyclisation of **7** was effected by addition of 0.15 equiv. of $AlCl_3$ to the reaction mixture and refluxing it for 3 h. Compound **3** was obtained as a colourless powder in 66% yield after recrystallisation from diethyl ether–hexane. Dewar also reported[18d] that the anhydride, bis(boroxophenanthryl)ether **4**, could be formed in the solid state by heating **3**, but the formation of this compound was never proven unambiguously. Solution phase ^{1}H NMR spectra of **3**, recorded at 300 MHz in both $(CD_3)_2CO$ and $CDCl_3$, indicate

Table 3 Calculated (HF/6-31G(d,p)) minimum and maximum values of the molecular electrostatic potential (ESP) on selected atoms in **3**. Data are also provided for benzene for comparison

Compound	Atom	$ESP_{max/min}$/kJ mol^{-1}
syn-**3**	Endocyclic O	−28
	B	+98
	O aromatic ring[a]	−32
	B aromatic ring[b]	−52
Benzene	C	−84

[a] Aromatic ring to which endocyclic O atom is attached. [b] Aromatic ring to which B atom is attached.

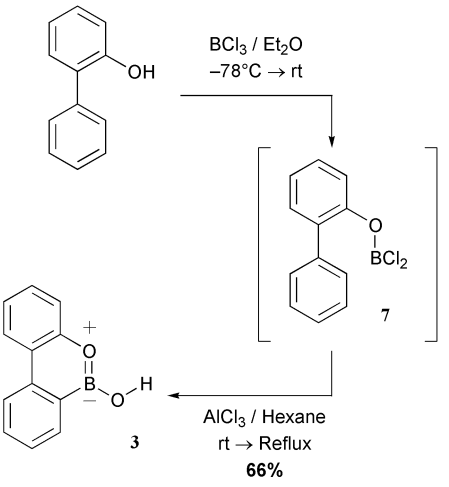

Scheme 2

that only **3** is present in solution, with no evidence for the formation of the anhydride **4**. This observation is in stark contrast to the behaviour[16] in solution of the closely related borazaaromatic 10-hydroxy-10,9-borazaphenanthrene **6**. Solution phase ^{1}H NMR spectra of this compound show that both the B-hydroxy compound and the corresponding anhydride are present in equilibrium. It is clear from our studies that **3** does not dehydrate to form the anhydride **4** in solution. However, a sample of the anhydride **4** can be prepared by heating **3** in the solid state for 2 h *in vacuo* (a strong signal at m/z 374 in the EI mass spectrum of the product confirms that the anhydride **4** is formed). However, when the material prepared in this manner is dissolved in $CDCl_3$, the 300 MHz ^{1}H NMR spectrum reveals that only **3** is present. It is therefore evident that rehydration of **4** occurs almost immediately in solution, making it impossible to record a ^{1}H NMR spectrum of the anhydride in $CDCl_3$ solution, *i.e.* anhydride **4** is clearly very unstable to hydrolysis.

Solid-state structure and reactivity

Crystals of 10-hydroxy-10,9-boroxophenanthrene **3** suitable for single crystal X-ray diffraction were grown by vapour diffusion of hexane into a solution of **3** in diethyl ether. The solid-state structure[22] of **3**, determined by single crystal X-ray diffraction, contains $R_2^2(8)$ hydrogen-bonded homodimers (Fig. 2), similarly to 10-hydroxy-10,9-borazaphenanthrene **6**,[16] and all eight molecules in the unit cell are involved in these cyclic hydrogen-bonded dimers. The two molecules within each [**3**·**3**] homodimer participate in two O–H···O hydrogen bonds. These two hydrogen bonds have the same H···O distance (1.96 Å), but their O–H···O angles differ significantly (157 *vs.* 176°). The donor oxygen atom associated with the less linear hydrogen bond displays a relatively short contact (3.14 Å) to a boron atom in the layer below. Unlike 10-hydroxy-10,9-borazaphenanthrene, which has two peripherally hydrogen-bonded molecules associated with each homodimer, boroxophenanthrene **3** has no free protons to interact in this manner. Stacks of the [**3**·**3**] homodimers propagate along the crystallographic *b* axis.

As a result of its instability to hydrolysis, single crystals of **4** could not be grown by vapour diffusion methods. However, the solid-state structure of **4** has been determined[23] previously by Sheldrick *et al.* using single crystals prepared by sublimation. Recognising that the crystal structure of a reaction product generated directly *via* a solid-state reaction is not necessarily the same as the crystal structure of the same material in crystals grown by crystal growth techniques, we wished to investigate the nature of the solid-state reaction that occurs when **3** is heated to form **4**. Thus, a sample of **3** was heated

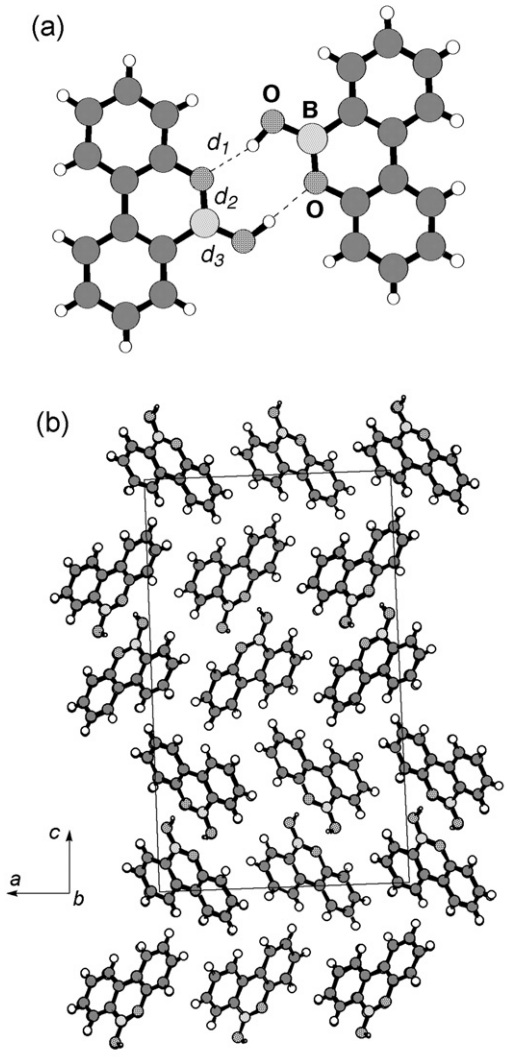

Fig. 2 (a) Ball and stick representation of the [**3**·**3**] homodimer within the solid-state structure of **3**. Dashed lines represent hydrogen bonds. Distances and bond lengths: $d_1 = 1.91$, $d_2 = 1.39$, $d_3 = 1.35$ Å. (b) Projection of the solid-state structure of **3** along the crystallographic *b* axis. The projection of the unit cell is represented by the solid lines.

until the transformation to **4** was complete and the powder X-ray diffraction pattern of this sample was used to determine the solid-state structure of this material. The structure of **4** generated through the solid-state reaction of **3** (Fig. 3) appears to be consistent with the structure reported[23] previously. However, structure refinement from the powder diffraction data does not allow us to determine with certainty whether the structure is ordered or disordered, since both models fit the diffraction data equally well (see Experimental section).

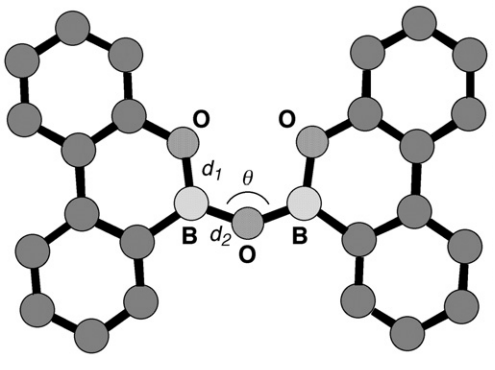

Fig. 3 Ball and stick representation of the molecular structure **4** determined from powder X-ray diffraction data. Bond lengths and angles: $d_1 = 1.40$, $d_2 = 1.38$ Å; $\theta = 139°$.

The observed melting points of both 10-hydroxy-10,9-boroxophenanthrene **3** and bis(boroxophenanthryl)ether **4** are 214–216 °C. In order to determine the nature of the solid-state transformation from **3** to **4**, heating experiments were carried out using differential scanning calorimetry (DSC). On heating a sample of **3** at 100 °C min^{-1}, an endothermic process takes place [Fig. 4(a)] between 130 and 160 °C, corresponding to the transformation of **3** to **4**. A second endotherm occurs at 215–225 °C, with an onset temperature of 208 °C, corresponding to melting of **4**. On cooling at 100 °C min^{-1}, the sample recrystallises at 165 °C. Once the sample had cooled to ambient temperature, it was reheated to 250 °C at 20 °C min^{-1} [Fig. 4(b)]. The endotherm at 215–225 °C is still present, but the endotherm observed in the previous experiment between 130 and 160 °C is no longer seen, indicating that, in contrast to the situation in solution, the anhydride **4** remains stable in the solid state.

In this work, we have employed two different techniques, thermogravimetric analysis (TGA) and powder X-ray diffraction (PXRD), to monitor the solid-state transformation from **3** to **4** as a function of time. It is crucial to recognize that each of these techniques probes a different aspect of the system (and, in the present context, monitors the change in a different aspect of the system as a function of time). Moreover, neither

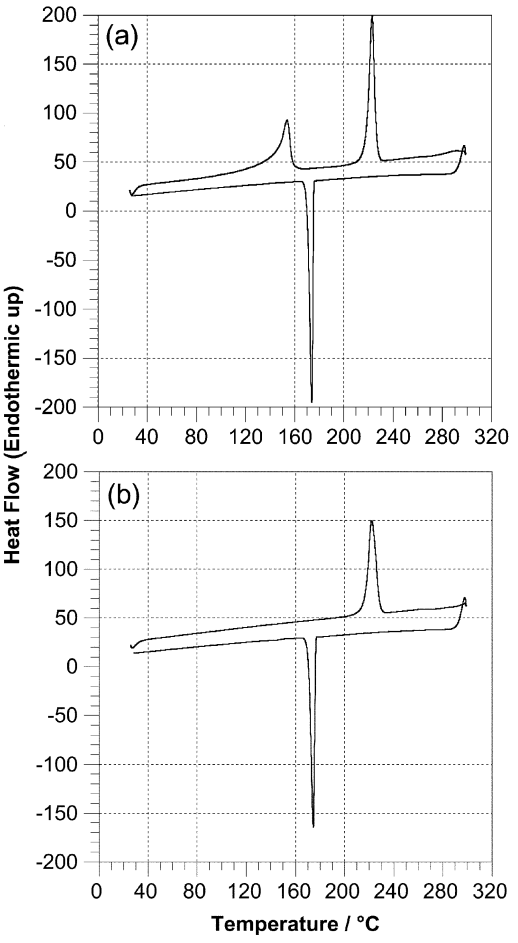

Fig. 4 (a) DSC plot (heat flux *vs.* temperature) recorded on heating a sample of **3** from room temperature to 250 °C at 100 °C min^{-1}. The onset of the solid-state transformation from **3** to **4** is clearly visible at *ca.* 145 °C, and the sample melts at *ca.* 215 °C. (b) DSC plot (heat flux *vs.* temperature) recorded on reheating the same sample from room temperature to 250 °C at 100 °C min^{-1}. The exotherm at *ca.* 145 °C is now absent.

of these techniques actually probes the chemical reaction from **3** to **4** directly. Specifically, the isothermal TGA experiment monitors the loss of mass of the sample as a function of time, arising in the present case from liberation of H_2O from the solid sample to the vapour phase. We emphasize that the rate of liberation of H_2O from the solid to the vapour phase is not necessarily equal to the rate of production of H_2O within the crystals of the reactant **3**, and therefore the rate of mass loss does not necessarily reflect the rate of the chemical transformation from **3** to **4** within the crystal (the rate of mass loss would equal the rate of the chemical transformation only in the limiting case in which the rate of release of H_2O molecules from the crystal is substantially faster than the chemical transformation that produces H_2O). On the other hand, the PXRD experiment monitors the changing identity of crystalline phases present during the solid-state transformation, and here we recall that, in order to observe sharp lines in the PXRD pattern, it is necessary that crystalline particles of sufficient size are present. Henceforth, we use $\{\ \}_3$ and $\{\ \}_4$ to denote the crystalline phases characteristic of **3** and **4**, respectively, and we use **3** and **4** to refer to the actual chemical identity of the molecules present within these crystalline phases. Again, the growth of crystalline particles of the product phase $\{\mathbf{4}\}_4$ of sufficient size to give a PXRD pattern characteristic of this phase need not necessarily proceed at the same rate as the actual chemical transformation from **3** to **4** within the parent crystal structure of **3** (*i.e.* $\{\mathbf{3}\}_3$). In particular, at sufficiently low values of the extent of reaction α, molecules of **4** produced by the chemical reaction can be accommodated within the reactant crystal structure of **3** (representing a solid solution $\{\mathbf{3},\mathbf{4}\}_3$, and possibly also containing H_2O molecules produced from the reaction). At this stage, no amount of the product phase $\{\mathbf{4}\}_4$ will actually be present, even though molecules of **4** have been produced by the chemical reaction, and powder X-ray diffraction will show no evidence for the presence of the product phase $\{\mathbf{4}\}_4$. Once the amount of **4** within the crystal structure of **3** exceeds its solid-state solubility, phase segregation will occur to produce **4** in its own crystal structure $\{\mathbf{4}\}_4$. It is only when crystalline particles of sufficient size have been generated in this way that the existence of $\{\mathbf{4}\}_4$ will be evident in the PXRD pattern. The proposed scheme describing the solid-state transformation of **3** to **4** is shown in Fig. 5, and summarizes the points discussed above. It is clear from this scheme that TGA and PXRD experiments separately probe processes I and II, respectively. Furthermore, as these processes occur in parallel, the kinetic and mechanistic aspects of these two processes should, in general, be independent of each other. Thus, processes I and II may occur at different rates and may be based on different mechanisms (for example, in terms of the required structural reorganization within the solid). Although the rates of both processes I and II will, in general, be different from the rate of the actual chemical transformation from **3** to **4**, we note that, as both processes follow sequentially from the chemical transformation, the rates of both processes will nevertheless depend on the rate of the chemical transformation.

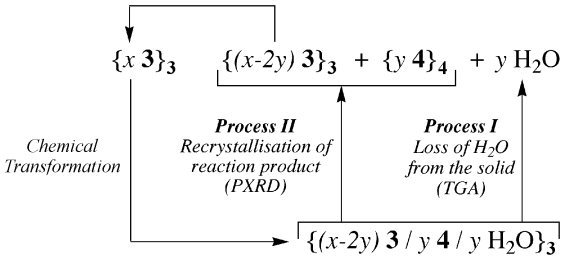

Fig. 5 Schematic representation of the solid-state transformation of **3** to **4**. The products shown refer to the situation at an extent of reaction $\alpha = 2y/x$, with $2y \leq x$. The notations $\{\ \}_3$ and $\{\ \}_4$ denote compounds located in the crystal structures of **3** and **4**, respectively.

During the chemical transformation from **3** to **4**, one molecule of water is lost for every two molecules of **3**, corresponding to a total mass loss at 4.6% from the sample. In a typical isothermal TGA experiment, a known mass of **3** was heated to a pre-set temperature between 55 and 100 °C and then held at this temperature until the measured mass reached 95.4% of its original value. This type of isothermal TGA experiment was then repeated at several different temperatures in order to investigate the effect of temperature on the rate of mass loss. As expected [Fig. 6(a)], the rate of mass loss decreases with decreasing temperature. However, at temperatures below 75 °C, the reaction rate decreases dramatically. EI mass spectra of the materials formed in these experiments show, in all cases, strong signals at m/z 374, indicative of the expected anhydride product **4**. A plot of the fractional extent of reaction, α, *vs.* time, t, for each temperature illustrates the variation of the reaction rate as the temperature is varied from 55 to 100 °C. The end of the reaction (*i.e.* $\alpha = 1$) is defined as the point at which a total mass loss of 4.6% is reached. Further isothermal heating beyond this point results in a continued mass loss, but at a significantly reduced rate, probably as a result of sublimation. Indeed, in separate experiments, sublimation is observed when a sample of **3** is heated under vacuum. The kinetic data obtained at each temperature were fitted using the Avrami–

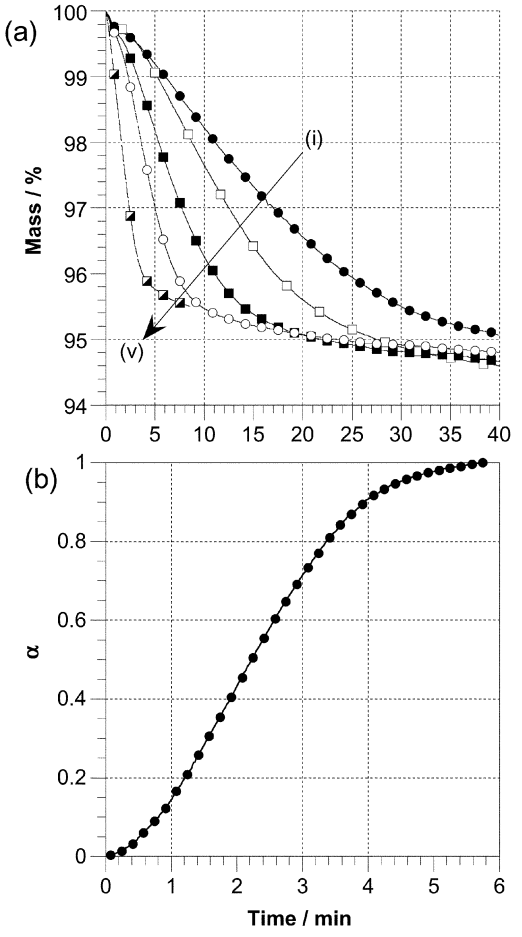

Fig. 6 (a) Thermogravimetric analysis (TGA) data (plotted as mass loss *vs.* time) for the solid-state transformation of **3** to **4**. Each experiment was carried out by heating a sample of **3** isothermally at (i) 70, (ii) 75, (iii) 80, (iv) 90 and (v) 100 °C. A mass loss of 4.6% corresponds to the loss of one mole of water for every two moles of **3** and hence to the formation of one mole of the anhydride, **4**. (b) TGA data obtained by heating a sample of **3** at 100 °C plotted as extent of reaction (α) *vs.* time. The solid line represents the best fit of the Avrami–Erofe'ev equation (with $n = 2$) to the experimental data.

Erofe'ev equation[24] (eqn. 1), which is commonly used to describe solid-state reactions.

$$\alpha(t) = 1 - \exp(-kt^{n}) \quad (1)$$

where $\alpha(t)$ = fractional extent of reaction k = rate constant and n = integer. A typical fit of the experimental TGA data to the Avrami–Erofe'ev equation is shown in Fig. 6(b).

Empirically, it has been found that the value of n usually lies between 2 and 4 and is described as comprising two components, β and λ. The component β represents the number of steps involved in formation of nuclei and usually takes the value 0 (corresponding to instantaneous nucleation) or 1 (single step nucleation). The component λ represents the number of dimensions in which growth of the nuclei occurs and may take a value of 1, 2 or 3. In this case, the best fit of the experimental data is obtained for $n = 2$. The data recorded at temperatures above 70 °C can all be fitted to the Avrami–Erofe'ev equation using the same value of n, within experimental error. The values of the rate constant k extracted at different temperatures were then analysed using a variant of the Arrhenius equation. A plot of $\ln k$ *vs.* $1/T$ (Fig. 7) has a gradient of $-E_a/R$, where E_a is the activation energy for the mass loss from the solid. Applying a linear fit to the data presented in Fig. 6 affords a value of 140 kJ mol^{-1} for the activation energy of the observed process.

In order to determine the rate of structural change, the transformation from **3** to **4** was studied using variable temperature powder X-ray diffraction (PXRD). An initial diffraction pattern was recorded at room temperature and the sample was then heated rapidly to the desired temperature. Further diffraction data were then recorded at regular time intervals at this temperature. This procedure was repeated at several different temperatures. In each case, the loss of the peaks characteristic of the reactant phase **3** [Fig. 8(a, i)] coincides exactly with the growth of a new set of peaks characteristic of the product phase **4** [Fig. 8(a, ii)]. The PXRD pattern recorded using a sample of the material recovered from the TGA heating experiments described above is identical to the diffraction pattern obtained at the end of the high temperature PXRD experiments. The structural change observed by PXRD was reproducible and occurred within 1 h at 100 °C. The rate of change in the identity of the crystalline phases present may be followed by observing the loss of reflections characteristic of the reactant phase $\{\mathbf{3}\}_3$, and the concurrent growth of reflections characteristic of the product phase $\{\mathbf{4}\}_4$. Fig. 8(b) shows the

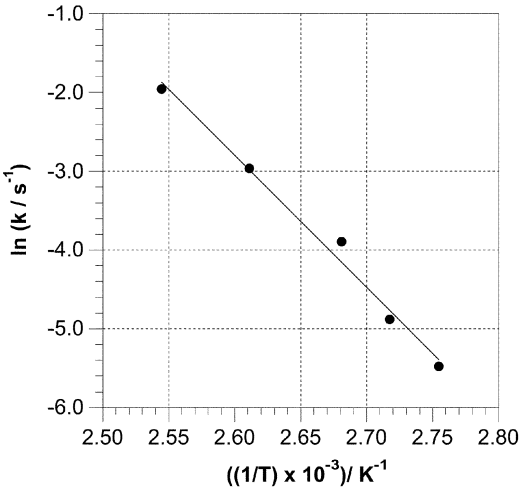

Fig. 7 Arrhenius plot ($\ln k$ *vs.* $1/T$) for the mass loss due to the solid-state transformation of **3** to **4** at temperatures higher than 70 °C. The data are fitted by a straight line, the gradient of which is $-E_a/R$, where E_a is the energy of activation for the process (E_a = 140 kJ mol^{-1}).

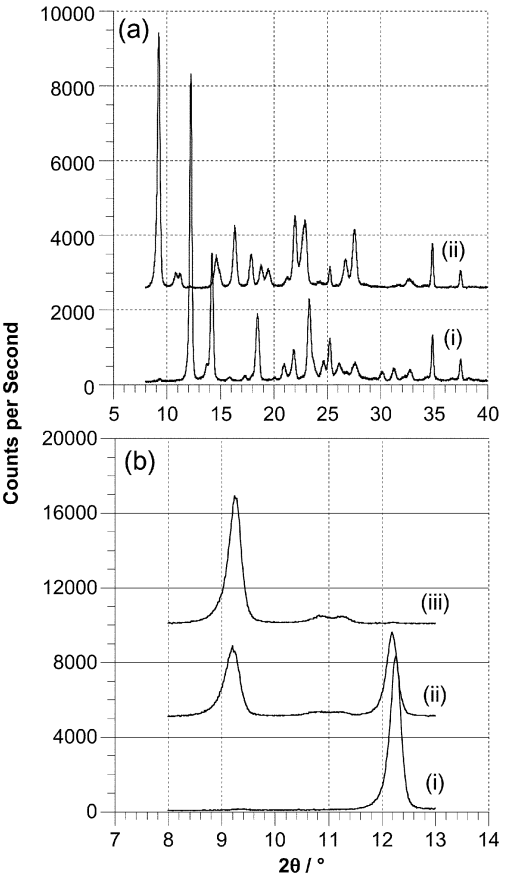

Fig. 8 (a) The structural changes that occur during the solid-state transformation from **3** to **4** are illustrated by a change in the powder X-ray diffraction patterns recorded (i) at the start of the experiment and (ii) after heating at 100 °C for 120 min. (b) The solid-state reaction can be followed readily using the reflections in the range $8 \leq 2\theta \leq 13°$. The changes in this region of the diffraction pattern are illustrated (i) at the start of the experiment, (ii) after heating at 100 °C for 60 min and (iii) after heating at 100 °C for 120 min.

PXRD pattern in the range $8 < 2\theta < 13°$ recorded before, during and after heating. As the peaks in this region are particularly well resolved, they were used to follow the course of the reaction. A graph of peak intensity *vs.* time (Fig. 9) demonstrates that the product phase $\{\mathbf{4}\}_4$ is formed more rapidly at higher temperatures, as expected. Although the reaction reaches completion within 2 h at 80 °C and above, at lower temperatures, the reaction rate decreases significantly and some amount of the reactant phase $\{\mathbf{3}\}_3$ is still present, even after 18 h below 60 °C. The kinetic data obtained from the PXRD experiments can also be fitted to the Avrami–Erofe'ev equation. In this case, the best fit to the experimental data is obtained when $n = 1$, in contrast to the TGA data, which were best fitted using $n = 2$. This difference can be explained by recalling that the two different techniques (TGA and PXRD) actually observe different aspects of the solid-state transformation (processes I and II respectively) and, as discussed above, the kinetic and mechanistic aspects of these processes are not necessarily related to each other. We note that the PXRD data provide no evidence for the existence of any intermediate solid phases other than $\{\ \}_3$ and $\{\ \}_4$, in support of the scheme shown in Fig. 5. The fact that the rate of loss of the reactant crystalline phase $\{\ \}_3$ and the rate of generation of the product crystalline phase $\{\ \}_4$ are comparable (from the PXRD data, see Fig. 8) is also consistent with the suggestion that no intermediate phases are involved in the solid-state transformation. From comparison of the TGA and PXRD results (for example, compare Fig. 6(b) [TGA] and Fig. 9(a) [PXRD] for the

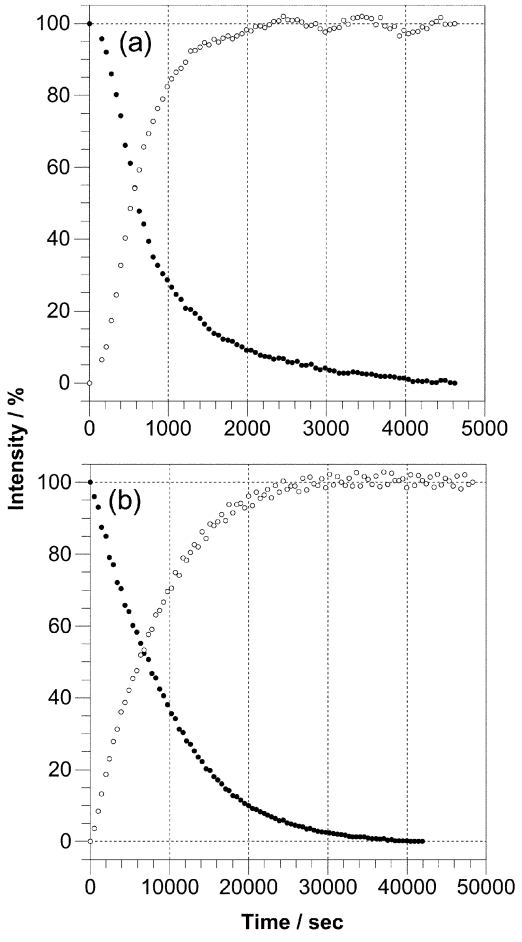

Fig. 9 Powder X-ray diffraction data for the solid-state transformation of **3** to **4** recorded at (a) 100 and (b) 80 °C. The data are plotted as peak intensity *vs.* time. Open circles represent the data for the reflection at $2\theta = 9°$ (from **4**) and filled circles represent the data for the reflection at $2\theta = 12°$ (from **3**). Note the different scale for the x axes in the two plots. The data give an excellent fit to the Avrami–Erofe'ev equation with $n = 1$.

transformation at 100 °C), it is clear that the liberation of H_2O from the solid (process I) occurs substantially faster (by about one order of magnitude at 100 °C) than the production of the crystalline phase of the product $\{\mathbf{4}\}_4$ (process II). As with many solid-state reactions, the scheme shown in Fig. 5 implies that a solid solution [represented as $\{(x-2y)\,\mathbf{3}/y\,\mathbf{4}/y\,H_2O\}_3$ in Fig. 5 is formed intially within the crystal structure of the reactant phase, followed by recrystallization (phase segregation) of the reactant [$\{\mathbf{3}\}_3$] and product [$\{\mathbf{4}\}_4$] phases. However, our results provide no information on the actual solubility of molecules of **4** within the crystal structure of the reactant phase $\{\ \}_3$, and therefore provide no information on the value of the extent of reaction α at which phase segregation occurs.

Solution phase reactivity

Thus far, the solid-state behaviour of 10-hydroxy-10,9-boroxophenanthrene **3** has been shown to be largely identical to that of the analogous borazaaromatic compound **6**. However, investigation of the solution phase reactivity of boroxophenanthrene **3** reveals several significant differences. The ^{1}H NMR spectrum of **3** was discussed above and is in marked contrast to that of 10-hydroxy-10,9-borazaphenanthrene **6**. It is already established that 10-hydroxy-10,9-borazaphenanthrene reacts slowly with other alcohols, such as benzyl alcohol, to form the corresponding alkoxy esters. In order to compare the solution phase reactivities of **3** and **6**, we attempted to follow the reaction between **3** and 4-methylbenzyl alcohol **8** [Scheme 3(a)] in solution using ^{1}H NMR spectroscopy. Equimolar amounts of **3** and **8** were dissolved in $CDCl_3$, and stirred over 4 Å molecular sieves. Then, 300 MHz ^{1}H NMR spectra of this solution were recorded at regular intervals. After approximately 3 min, the reaction had reached almost 60% completion, but then showed a significant decrease in rate. This observation indicates that nucleophilic attack of benzyl alcohol at boron is an inherently fast reaction, but suggests that the water formed during the reaction quickly overwhelms the molecular sieves and acts to slow the formation of the ester **9**. In order to eliminate this problem, we set up a "transesterification" equilibrium between 10-(4-methylbenzyloxy)-10,9-boroxo phenanthrene **9** and a second nucleophile, 4-*tert*-butylbenzyl alcohol **10** [Scheme 3(b)]. In this case, no water is formed during the reaction and we would therefore expect to observe the reaction without any decrease in rate due to hydrolysis of the ester. 4-*tert*-butylbenzyl alcohol was chosen as, in terms of nucleophilicity, it is similar to 4-methylbenzyl alcohol. Hence, we anticipated that the reaction rate observed would simply be a manifestation of the electrophilicity of the boron atom, rather than any other factors such as the nucleophilicity of the alcohol. The methyl- and *tert*-butyl-substituted benzyl alcohols also have convenient resonances in their ^{1}H NMR spectra which aid the interpretation of the equilibrium process by ^{1}H NMR spectroscopy. A sample of 10-(4-methylbenzyloxy)-10,9-boroxophenanthrene **9** was prepared by stirring a solution of **3** and 4-methylbenzyl alcohol **8** over 4 Å molecular sieves in $CDCl_3$ under N_2 for 2 days. Once ^{1}H NMR spectroscopy indicated that the condensation

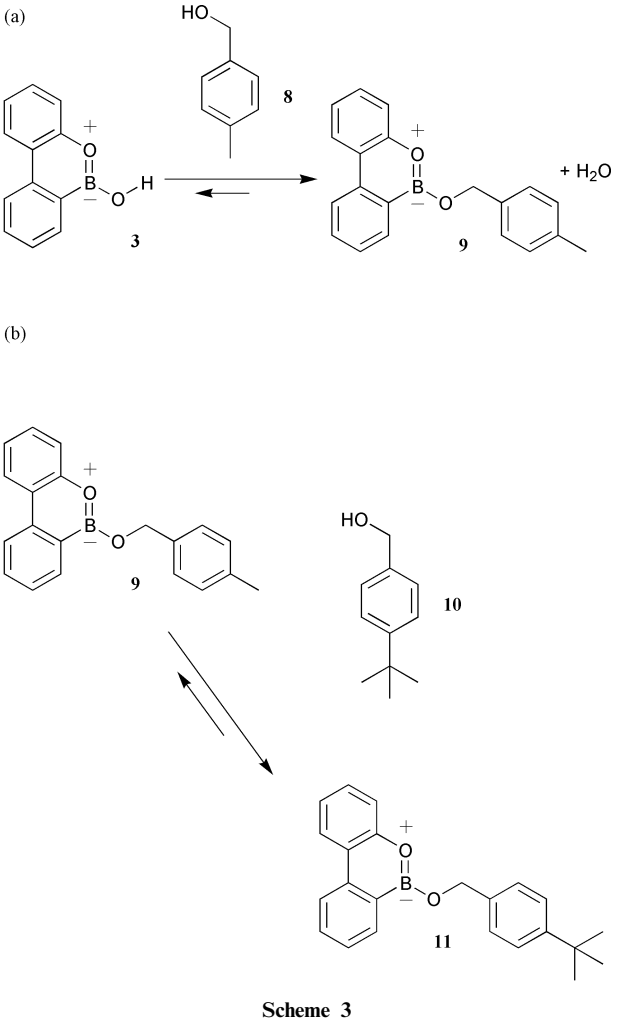

Scheme 3

reaction had gone to completion, the molecular sieves were removed and an equimolar amount of 4-*tert*-butylbenzyl alcohol **10** was added. Variable temperature ^{1}H NMR studies of the equilibration reaction indicated that equilibrium is reached within 3 min, even at $-40\,^{\circ}$C.

Conclusions

These experiments demonstrate conclusively that the solution phase chemistry of 10-hydroxy-10,9-boroxophenanthrene **3** is markedly different from that of the corresponding borazaaromatic **6**. Compound **3** reacts with itself on heating only in the solid state, whereas **6** forms the corresponding homoanhydride both in the solid state and in solution. In the case of **3**, the solid-state dehydration reaction to form the homoanhydride **4** can be followed readily using techniques such as TGA and PXRD. Although **3** does not react with itself in the solution phase, it does react rapidly and reversibly with other nucleophiles. This reactivity is markedly different from that of **6**, which exists in equilibrium with its anhydride in the solution phase, and does not readily undergo reactions with nucleophiles. We aim to exploit this complementary reactivity in developing a series of bifunctional building blocks whose assembly into large, complex structures is programmed by the complementary reversible reaction of boroxo- and borazaaromatics.

Experimental

General procedures

Diethyl ether was dried by refluxing over sodium–benzophenone ketyl under a N_2 atmosphere and collected by distillation. Hexane was dried by heating under reflux over calcium hydride and distilled under N_2. All other solvents and reagents were used as received. Thin layer chromatography (TLC) was performed on aluminium or glass plates coated with Merck Kieselgel 60 F_{254}. Developed plates were scrutinised under a UV lamp. Melting points were determined on an Electrothermal 9200 melting point apparatus, and are uncorrected. Infrared spectra were recorded on a Perkin Elmer Paragon 1000 FTIR spectrometer using samples prepared as KBr discs. ^{1}H NMR spectra were recorded on either a Bruker AC300 (300 MHz) or a Bruker DRX500 (500MHz) spectrometer using the deuterated solvent as the lock and the residual solvent peak as the internal reference. ^{13}C NMR spectra were recorded on a Bruker AC300 (75.5 MHz) spectrometer using the PENDANT sequence, also using the deuterated solvent as the lock and the residual solvent peak as the internal reference. ^{11}B NMR spectra were recorded on a Bruker DRX500 (160.4 MHz) spectrometer, again using the deuterated solvent as the lock and trimethyl borate as the internal reference. Electron impact mass spectrometry (EIMS) and high resolution mass spectrometry (HRMS) were carried out on a VG Prospec mass spectrometer. Powder X-ray diffraction patterns were recorded on a variable temperature Siemens D5005 diffractometer. All elemental analyses (EA) were carried out either by SACS, University of North London or at the University of Birmingham. Thermogravimetric analysis (TGA) experiments (typical sample mass *ca.* 10 mg) were performed on a Perkin Elmer TGA 6 thermogravimetric analyzer, and differential scanning calorimetry (DSC) experiments (typical sample mass *ca.* 5 mg) were carried out using a Perkin Elmer Pyris 1 differential scanning calorimeter.

Computational studies

Electronic structure calculations were performed on a Silicon Graphics O2 workstation using SPARTAN.[25] All calculations were performed at the HF/6-31G(d,p) level of theory and all molecular structures were optimised fully.

Determination of the solid-state structure of 4 from powder X-ray diffraction data

The powder X-ray diffraction pattern of **4** was recorded at $22\,^{\circ}$C on Station 2.3 at the Synchrotron Radiation Source, Daresbury Laboratory, using a wavelength of 1.4000 Å. A capillary sample holder was used, with the data recorded over the 2θ range 5 to 60° in steps of 0.01°. The powder X-ray diffraction pattern was indexed by the program ITO,[26] giving the monoclinic unit cell: $a = 9.357$, $b = 15.248$, $c = 6.407$ Å, $\beta = 99.16°$. On the basis of systematic absences, the space group is assigned as $P2_1/c$, and density considerations suggest that there are two molecules of **4** in the unit cell. In space group $P2_1/c$ (which has 4 general positions), this situation implies that there is disorder of the molecules of **4** in the crystal structure. To simplify the structural analysis, structure solution was carried out initially in space group $P2_1$ (with one molecule of **4** in the asymmetric unit), with a view to exploring subsequently whether the description in the higher symmetry space group $P2_1/c$ would be more appropriate.

Structure solution was carried out directly from the powder diffraction data using the genetic algorithm (GA) method,[27] which is based on the direct-space strategy for structure solution.[28] In this strategy, trial crystal structures are sampled in direct space, with the "quality" of each trial structure assessed by directly comparing the powder diffraction pattern calculated for the trial structure and the experimental powder diffraction pattern. In the present work, this comparison is made using the powder profile *R*-factor R_{wp}. In the GA method, a population of trial structures is allowed to evolve subject to the normal rules and operations (mating, mutation and natural selection) that govern evolutionary systems.

In the GA structure solution calculation, the structural fragment comprised all non-hydrogen atoms of the molecule, which was constructed using standard bond lengths and bond angles. The two boroxophenanthrene ring systems were maintained as rigid units, with the molecular conformation defined by the two O–B–O–B torsion angles (variables τ_1 and τ_2) at the centre of the molecule. Thus, the structure is defined by 8 variables $\{x, y, z, \theta, \phi, \psi, \tau_1, \tau_2\}$, where $\{x, y, z\}$ refers to the position of the central oxygen atom, although in space group $P2_1$ the y coordinate may be fixed arbitrarily, representing a total of 7 structural variables. The GA calculation involved the evolution of 200 generations of a population of 100 structures. In each generation, 100 offspring (obtained from 50 pairs of parents) and 10 mutations were generated. In the evolution of the population, the value of R_{wp} for the best structure in the population dropped from *ca.* 38% in the first generation to *ca.* 21% in the final generation.

The best structure solution (lowest R_{wp} in the final generation) was taken as the starting model for Rietveld refinement using the GSAS program.[29] The positions of all non-hydrogen atoms were refined, with standard geometric restraints applied to bond lengths and bond angles, and a common isotropic displacement parameter was used for all atoms. In the final stages, a preferred orientation parameter was refined. The final Rietveld refinement gave $R_{wp} \approx 8\%$ and $R_p \approx 11\%$.

Following successful Rietveld refinement in space group $P2_1$, the possibility of describing the structure in the higher symmetry space group $P2_1/c$ was explored, recalling that this space group implies the introduction of disorder within the crystal structure. In particular, addition of an inversion centre to the structure refined in space group $P2_1$ corresponds to a model involving disorder only in the position of the central oxygen atom of the molecule of **4**, with this atom disordered between two sites of half occupancy, and in the occupancies of the heterocyclic O and B atom positions (half occupancy

of O and half occupancy of B in each case). These two positions of the central oxygen atom correspond to two different molecular orientations (related by a 180° flip), such that the positions of all atoms except the central oxygen atom are identical in the two molecular orientations. Rietveld refinement of this structural model in space group $P2_1/c$ was successful, and gave rise to an equally good fit to the powder diffraction data as the refinement discussed above in space group $P2_1$.

Syntheses

10-Hydroxy-10,9-boroxophenanthrene 3. 2-Phenylphenol (5.00 g, 29.4 mmol) was stirred at −78 °C (liquid N_2–ethyl acetate) in dry diethyl ether (50 cm^3) under a N_2 atmosphere. A solution of boron trichloride (1 M in hexane) (35.3 cm^3, 35.3 mmol) was added dropwise whilst keeping the temperature below −70 °C. Once the addition was complete, the mixture was allowed to warm to room temperature over 2 h and volatile solvents were removed under reduced pressure (1 mm Hg). Dry hexane (60 cm^3) and anhydrous aluminium chloride (0.6 g, 4.4 mmol) were added to the solid residues and the reaction mixture was then heated at reflux. After 3 h, the mixture was allowed to cool, filtered through Celite® 521 filter agent and the solid residue washed with ether (50 cm^3). The filtrate was quenched with water (50 cm^3) and the aqueous phase extracted with ether (3×100 cm^3). The combined organic extracts were dried ($MgSO_4$) and concentrated under reduced pressure. The resulting solid was recrystallised (ether–hexane) to afford **3** as colourless crystals (3.10 g, 56%); found: C, 73.7; H, 4.8; calcd. for $C_{12}H_9BO_2$: C, 73.5; H, 4.6%; m.pt.: 214–216 °C (as anhydride) (lit: 205–206 °C[17a]); IR (KBr): ν_{max}/cm^{-1} 3278br (OH); δ_H (300 MHz, $CDCl_3$) 8.12–8.20 (3H, m), 8.04–8.11 (1H, m), 7.48–7.76 (1H, m), 7.44–7.53 (1H, m), 7.34–7.42 (1H, m), 7.20–7.31 (1H, m), 4.72 (1H, br s); δ_C [75.5 MHz, $(CD_3)_2CO$] 152.5 (quat, Ar), 141.1 (quat, Ar), 134.3 (CH, Ar), 133.2 (CH, Ar), 129.8 (CH, Ar), 128.0 (CH, Ar), 124.5 (CH, Ar), 123.7 (quat, Ar), 123.3 (CH, Ar), 122.5 (CH, Ar) and 120.2 (CH, Ar); δ_B (160.4 MHz; $(CD_3)_2CO$) 9.49; MS (70 eV, EI) m/z: 196 (M^+, 100) and 152 (10%); HRMS found: 196.06980; calcd for $C_{12}H_9BO_2$: 196.06956.

Bis-boroxophenanthryl ether 4. 10-Hydroxy-10,9-boroxophenanthrene (1.00 g, 5.1 mmol) was heated to 100 °C under reduced pressure for 2 h to afford bis-boroxophenanthryl ether (1.60 g, 4.3 mmol, 84%). Some sample was lost to sublimation, as also observed during the TGA experiments. Solution phase NMR spectra of **4** could not be recorded, as this compound is very unstable to hydrolysis. Mass spectra were obtained by dry application of the sample on to the probe tip; m.pt.: 214–216 °C (lit: 205–206 °C[17]); MS (70 eV, EI) m/z: 374 (M^+, 73) and 198 (100%); HRMS found: 374.12673; calcd for $C_{24}H_{16}B_2O_3$: 374.12856.

10-(4-Methylbenzyloxy)-10,9-boroxophenanthrene 9. 10-Hydroxy-10,9-boroxophenanthrene (19.6 mg, 0.1 mmol) and 4-methylbenzyl alcohol (12.2 mg, 0.1 mmol) were rigorously dried under reduced pressure before dissolving in $CDCl_3$ (pre-dried over 4 Å molecular sieves, 1 cm^3). The mixture was stirred over 4 Å molecular sieves for a further 72 h. The solvent was removed under reduced pressure to afford **9** as a white solid (30 mg, 99%); m.pt.: 82–84 °C; δ_H (300 MHz, $CDCl_3$) 8.09–8.20 (3H, m), 7.65–7.72 (1H, m), 7.39–7.46 (2H, m), 7.34–7.36 (2H, m), 7.18–7.25 (4H, m), 5.35 (2H, s, CH_2) and 2.36 (3H, s, CH_3); δ_C (75.5 MHz, $CDCl_3$) 151.4 (quat, Ar), 140.2 (quat, Ar), 137.4 (quat, Ar), 136.8 (quat, Ar), 133.6 (CH, Ar), 132.8 (CH, Ar), 132.4 (CH, Ar), 129.5 (CH, Ar), 129.3 (CH, Ar), 129.0 (CH, Ar), 127.4 (CH, Ar), 127.3 (CH, Ar), 123.8 (CH, Ar), 123.3 (quat, Ar), 122.9 (CH, Ar), 121.6 (CH, Ar), 119.9 (CH, Ar), 65.3 (CH_2) and 21.4 (CH_3); MS (70 eV, EI) m/z: 300 (M^+, 100) and 285 (36%); HRMS found: 300.16645; calcd for $C_{20}H_{17}BO_2$: 300.16601.

10-(4-*tert*-Butyl)benzyloxy-10,9-boroxophenanthrene 11. 10-Hydroxy-10,9-boroxophenanthrene (58.8 mg, 0.3 mmol) and 4-*tert*-butylbenzyl alcohol (49.3 mg, 0.3 mmol) were dried thoroughly under reduced pressure before being dissolved in $CDCl_3$ (pre-dried over 4 Å molecular sieves, 1 cm^3). The mixture was stirred over 4 Å molecular sieves for a further 72 h. The solvent was removed under reduced pressure to afford **11** as a white solid (103 mg, 100%); m.pt.: 70–72 °C; δ_H (300 MHz, $CDCl_3$) 8.15 (2H, d, $^3J = 9$ Hz), 7.67–7.73 (1H, m), 7.30–7.54 (6H, m), 7.15–7.28 (3H, m), 5.38 (2H, s), 1.35 (9H, s); δ_C (75.5 MHz, $CDCl_3$) 151.4 (Ar), 150.5 (Ar), 140.1 (Ar), 136.6 (Ar), 133.5 (Ar), 132.2 (Ar), 128.9 (Ar), 127.2 (Ar), 127.0 (Ar), 125.4 (Ar), 125.2 (Ar), 123.6 (Ar), 122.7 (Ar), 121.4 (Ar), 119.8 (Ar), 65.0 (CH_2), 34.5 (quat ^{t}Bu) and 31.3 (CH_3, ^{t}Bu); MS (70 eV, EI) m/z: 342 (M^+, 100) and 285 (36%); HRMS found: 342.17980; calcd for $C_{23}H_{23}BO_2$: 342.17911.

Acknowledgements

We thank the Engineering and Physical Sciences Research Council and the Universities of Birmingham and St Andrews for financial support.

References and notes

1 (*a*) L. M. Greig and D. Philp, *Chem. Soc. Rev.*, 2001, **30**, 287; (*b*) D. Philp and J. F. Stoddart, *Angew. Chem., Int. Ed. Engl.*, 1996, **35**, 1155; (*c*) D. S. Lawrence, T. Jiang and M. Levett, *Chem. Rev.*, 1995, **95**, 2229; (*d*) J. S. Lindsey, *New J. Chem.*, 1991, **15**, 153; (*e*) G. M. Whitesides, J. P. Mathias and C. T. Seto, *Science*, 1991, **254**, 1312.
2 B. Alberts, D. Bray, J. Lewis, M. Raff, K. Roberts and J. D. Watson, *Molecular Biology of the Cell*, Garland, New York, 2nd edn., 1989, p. 84.
3 A. Klug, *Angew. Chem., Int. Ed. Engl.*, 1983, **22**, 565.
4 L. Stryer, *Biochemistry*, W. H. Freeman, New York, 3rd edn., 1988, p. 852.
5 (*a*) A. Zafar and A. D. Hamilton, in *Current Challenges in Large Supramolecular Assemblies*, ed. G. Tsoucaris, Kluwer Academic Publishers, London, 1999, p. 67; (*b*) J. Yang, J.-L. Marendaz, S. J. Geib and A. D. Hamilton, *Tetrahedron Lett.*, 1994, **35**, 3665; (*c*) C. T. Seto and G. M. Whitesides, *J. Am. Chem. Soc.*, 1993, **115**, 905; (*d*) F. Garcia-Tellado, S. J. Geib, S. Goswami and A. D. Hamilton, *J. Am. Chem. Soc.*, 1991, **113**, 9265; (*e*) J.-M. Lehn, M. Mascal, A. DeCian and J. Fisher, *J. Chem. Soc., Chem. Commun.*, 1990, 479.
6 (*a*) V. C. M. Smith and J.-M. Lehn, *Chem. Commun.*, 1996, 2733; (*b*) P. J. Stang, K. Chen and A. M. Arif, *J. Am. Chem. Soc.*, 1995, **117**, 8793; (*c*) R. Krämer, J.-M. Lehn and A. Marquis-Rigault, *Proc. Natl. Acad. Sci. U. S. A.*, 1993, **90**, 5394.
7 (*a*) A. E. Eschenmoser and C. E. Wintner, *Science*, 1977, **196**, 1410; (*b*) R. B. Woodward, *Pure Appl. Chem.*, 1973, **33**, 145.
8 R. W. Armstrong, J.-M. Beau, S. H. Cheon, W. J. Christ, H. Fujioka, W.-H. Ham, L. D. Hawkins, H. Jin, S. H. Kang, Y. Kishi, M. J. Martinelli, W. W. McWhorter, Jr., M. Mizuno, M. Nakata, A. E. Stutz, F. X. Talamas, M. Taniguchi, J. A. Tino, K. Ueda, J. Uenishi, J. B. White and M. Yonaga, *J. Am. Chem. Soc.*, 1989, **111**, 7525.
9 S.-W. Tam-Chang, J. S. Stehouwer and J. Hao, *J. Org. Chem.*, 1999, **64**, 334.
10 T. D. James, K. R. A. Samankumara Sandanayake and S. Shinkai, *Angew. Chem., Int. Ed. Engl.*, 1996, **35**, 1910.
11 (*a*) S. J. Rowan, P. A. Brady and J. K. M. Sanders, *Angew. Chem., Int. Ed. Engl.*, 1996, **35**, 2143; (*b*) S. J. Rowan, P. A. Brady and J. K. M. Sanders, *Tetrahedron Lett.*, 1996, **37**, 6013; (*c*) P. A. Brady and J. K. M. Sanders, *Chem. Soc. Rev.*, 1997, **26**, 327; (*d*) S. J. Rowan, D. G. Hamilton, P. A. Brady and J. K. M. Sanders, *J. Am. Chem. Soc.*, 1997, **119**, 2578; (*e*) S. J. Rowan and J. K. M. Sanders, *Chem. Commun.*, 1997, 1407; (*f*) S. J. Rowan and J. K. M. Sanders, *J. Org. Chem.*, 1998, **63**, 1536.

12 (*a*) G. Ercolani, L. Mandolini, P. Mencarelli and S. Roelens, *J. Am. Chem. Soc.*, 1993, **115**, 3901; (*b*) G. Ercolani, *J. Phys. Chem. B*, 1998, **102**, 5699.
13 The first definition of the term *predisposition* can be found in: *Comprehensive Supramolecular Chemistry*, ed. J. L. Atwood, J. E. D. Davies, D. D. MacNicol and F. Vögtle, Elsevier, New York, 1996, vol. 9, p. 218. Sanders defines[11d] the term *predisposition* as "a strong conformational or structural preference expressed by the building block once incorporated into a larger structure".
14 (*a*) J. Ipaktschi, R. Hosseinzadeh and P. Schlaf, *Angew. Chem., Int. Ed.*, 1999, **38**, 1658; (*b*) J. Ipaktschi, R. Hosseinzadeh, P. Schlaf, E. Dreiseidler and R. Goddard, *Helv. Chim. Acta*, 1998, **81**, 1821.
15 P. J. Comina, D. Philp, B. M. Kariuki and K. D. M. Harris, *Chem. Commun.*, 1999, 2279.
16 K. D. M. Harris, B. M. Kariuki, C. Lambropoulos, D. Philp and J. M. A. Robinson, *Tetrahedron*, 1997, **53**, 8599.
17 (*a*) M. J. S. Dewar and R. Dietz, *Tetrahedron Lett.*, 1959, 21; (*b*) P. M. Maitlis *Chem. Rev.*, 1962, 223; (*c*) M. J. S. Dewar, in *Progress in Boron Chemistry*, ed. H. Steinberg and A. L. McCloskey, Macmillan, New York, 1964, vol. 1, p. 235; H. R. Snyder, A. J. Reedy and W. J. Lennary, *J. Am. Chem. Soc.*, 1958, **80**, 835; (*e*) W. J. Lennary and H. R. Snyder, *J. Am. Chem. Soc.*, 1960, **82**, 2172.
18 (*a*) B. M. Mikhailov and M. E. Kuimova, *J. Organomet. Chem.*, 1976, **116**, 123; (*b*) F. A. Davis and M. J. S. Dewar, *J. Org. Chem.*, 1968, **33**, 3324; (*c*) M. J. S. Dewar and R. Dietz, *Tetrahedron*, 1961, **15**, 26; (*d*) M. J. S. Dewar and R. Dietz, *J. Chem. Soc.*, 1960, 1344.
19 L. M. Greig, J. M. A. Robinson, P. J. Comina and D. Philo, *Tetrahedron*, submitted.
20 P.-Q. Löwdin, *Adv. Quantum Chem.*, 1970, **5**, 185.
21 P. R. Ashton, K. D. M. Harris, B. M. Kariuki, D. Philp, J. M. A. Robinson and N. Spencer, *J. Chem. Soc., Perkin Trans. 2*, 2001, 2166.
22 Single crystal X-ray diffraction data were recorded with $\lambda = 0.68850$ Å at the Synchrotron Radiation Source (Daresbury Laboratory) on Station 9.8, which is equipped with a Siemens SMART CCD diffractometer. The structure was solved using the program SHELXS (G. M. Sheldrick, SHELXS86, Program for the Solution of Crystal Structures, University of Göttingen, Germany, 1986) and refined using the program SHELXL (G. M. Sheldrick, SHELXL92, Program for the Refinement of Crystal Structures, University of Göttingen, Germany, 1993). The positions of all non-hydrogen atoms were refined with anisotropic displacement parameters, and all hydrogen atoms (except the hydroxyl hydrogen atom) were placed in calculated positions. Final refined $R_1 = 4.71\%$, $R_w = 13.05\%$. Crystal data for **1** at 150 K: $C_{12}H_9BO_2$, $M = 196.00$ g mol^{-1}, orthorhombic, space group $Pna2_1$, $a = 14.683(2)$, $b = 5.1589(7)$, $c = 24.502(3)$ Å, $V = 1856.0(4)$ Å^3, $Z = 8$, $D_c = 1.403$ g cm^{-3}, $F(000) = 816$.
23 W. Maringgele, A. Meller, M. Noltemeyer and G. M. Sheldrick, *Z. Anorg. Allg. Chem.*, 1986, **536**, 24.
24 W. E. Brown, D. Dollimore and A. K. Galwey, *Comprehensive Chemical Kinetics*, ed. C. H. Bamford and C. F. H. Tipper, Elsevier Scientific Publishing, Oxford, 1980, p. 57.
25 SPARTAN, version 5.1.3, Wavefunction Inc., Irvine, CA, 1998.
26 J. W. Visser *J. Appl. Crystallogr.*, 1969, **2**, 89.
27 (*a*) B. M. Kariuki, H. Serrano-González, R. L. Johnston and K. D. M. Harris, *Chem. Phys. Lett.*, 1997, **280**, 189; (*b*) K. D. M. Harris, R. L. Johnston and B. M. Kariuki, *Acta Crystallogr., Sect. A*, 1998, **54**, 632.
28 (*a*) K. D. M. Harris, M. Tremayne, P. Lightfoot and P. G. Bruce, *J. Am. Chem. Soc.*, 1994, **116**, 3543; (*b*) K. D. M. Harris and M. Tremayne, *Chem. Mater.*, 1996, **8**, 2554.
29 A. C. Larson and R. B. von Dreele, GSAS, Generalised Structure Analysis System, report LA-UR-86-748, Los Alamos National Laboratory, NM, 1987.